

Bioactive site-specifically modified proteins for 4D patterning of gel biomaterials

Jared A. Shadish¹, Gabrielle M. Benuska² and Cole A. DeForest^{1,3,4,5*}

Protein-modified biomaterials can be used to modulate cellular function in three dimensions. However, as the dynamic heterogeneous control over complex cell physiology continues to be sought, strategies that permit a reversible and user-defined tethering of fragile proteins to materials remain in great need. Here we introduce a modular and robust semisynthetic approach to reversibly pattern cell-laden hydrogels with site-specifically modified proteins. Exploiting a versatile sortase-mediated transpeptidation, we generate a diverse library of homogeneous, singly functionalized proteins with bioorthogonal reactive handles for biomaterial modification. We demonstrate the photoreversible immobilization of fluorescent proteins, enzymes and growth factors to gels with excellent spatiotemporal resolution while retaining native protein bioactivity. Localized epidermal growth factor presentation enables dynamic regulation over proliferation, intracellular mitogen-activated protein kinase signalling and subcellularly resolved receptor endocytosis. Our method broadly permits the modification and patterning of a wide range of proteins, which provides newfound avenues to probe and direct advanced cellular fates in four dimensions.

The extracellular matrix (ECM) directs cell function through a complex choreography of biomacromolecular interactions in a tissue-dependent manner. Far from static, this hierarchical milieu of biochemical and biophysical cues presented within the native cellular niche is both spatially complex and constantly changing^{1–3}. As these pericellular reconfigurations are vital for tissue morphogenesis, disease regulation and healing, *in vitro* culture platforms that recapitulate such dynamic environmental phenomena would be invaluable for fundamental studies in cell biology, as well as in the engineering of functional human tissue^{4,5}. Polymer-based hydrogels represent one such emerging and highly attractive class of *in vitro* cell culture constructs that offer promise for dynamic three-dimensional (3D) biological studies^{6–8}. Their high water content, tissue-like elasticity and facile transport of nutrients and waste render them ideal mimics of the cell's ECM, and their optical clarity permits the imaging of cell function to be performed non-destructively^{9–11}. Gel materials can be produced under mild, cytocompatible conditions that enable live-cell encapsulation and are readily formulated to contain user-defined chemical functionalities, mechanical properties and degradability^{12–14}. Through appropriately developed chemistries, such niche characteristics can be modified on demand to probe and direct cell fate in response to variable microenvironmental cues similar to those that comprise the native ECM^{15–17}.

To emulate the dynamic ECM biochemical heterogeneity *in vitro*, a significant effort has been dedicated towards the creation of an expansive library of chemical strategies for hydrogel alteration. Preliminary efforts in this regard largely focused on the exploitation of photochemical techniques to pattern bioactive small molecules and peptides spatially within synthetic hydrogel culture systems^{18–23}. Although such approaches proved successful in directing relatively simple cellular functions (such as adhesion and spreading), the ability to regulate more complex and dynamic decisions of fate using full-length proteins remains of prime interest^{24–27}. Although proteins represent a powerful tool in the quest to govern cell physiology, their fragility necessitates that careful consideration be given

to the chemistries employed as well as to the precise site of protein modification for material tethering to ensure a sustained stability and activity²⁸.

The installation of reactive groups onto the proteins required for biomaterial decoration has been performed almost exclusively through non-specific reactions with thiols and primary amines on endogenous cysteine and lysine residues²⁹. As these amino acids are not uniquely present on native proteins, bioconjugation of this type occurs randomly and stochastically to yield a heterogeneous collection of differently modified species. Such uncontrolled functionalization often leads to protein unfolding, loss of activity and supraphysiological doses required to elicit a cellular response. Coupled with batch-to-batch variability and ambiguous extents of modification, reproducibility problems dramatically hinder the laboratory and clinical translation of these ill-defined samples. Generalizable strategies to create homogeneous protein populations that can be used to modify a wide variety of biomaterial platforms while retaining native levels of bioactivity remain an open challenge.

Chemoenzymatic strategies have gained recent popularity for their unique ability to modify proteins in a manner that is site specific, selective and quantitative, and thereby permit the introduction of reactive chemical handles at defined locations^{30–34}. We identified the sortase-mediated transpeptidation modification strategy^{34,35} as one that could permit the installation of functional handles compatible with virtually any chemistry used for biomaterial formation or modification, which includes photoreactions that have previously proved beneficial for 4D biomaterial decoration. Sortase A, a calcium-assisted transpeptidase from *Staphylococcus aureus*, recognizes the sorting signal 'LPXTG' (where X is any amino acid) and forms an acyl-enzyme intermediate with the sorting signal's threonine residue, and simultaneously displaces other C-terminal amino acids³⁶. The resultant thioester intermediate can be nucleophilically displaced by reaction with the N-terminal amine of a polyglycine probe, and thereby conjugate a synthetic peptide onto the C terminus as it regenerates the sortase A enzyme. Critically, the polyglycine

¹Department of Chemical Engineering, University of Washington, Seattle, WA, USA. ²Department of Biochemistry, University of Washington, Seattle, WA, USA. ³Department of Bioengineering, University of Washington, Seattle, WA, USA. ⁴Institute for Stem Cell & Regenerative Medicine, University of Washington, Seattle, WA, USA. ⁵Molecular Engineering & Sciences Institute, University of Washington, Seattle, WA, USA. *e-mail: profcole@uw.edu

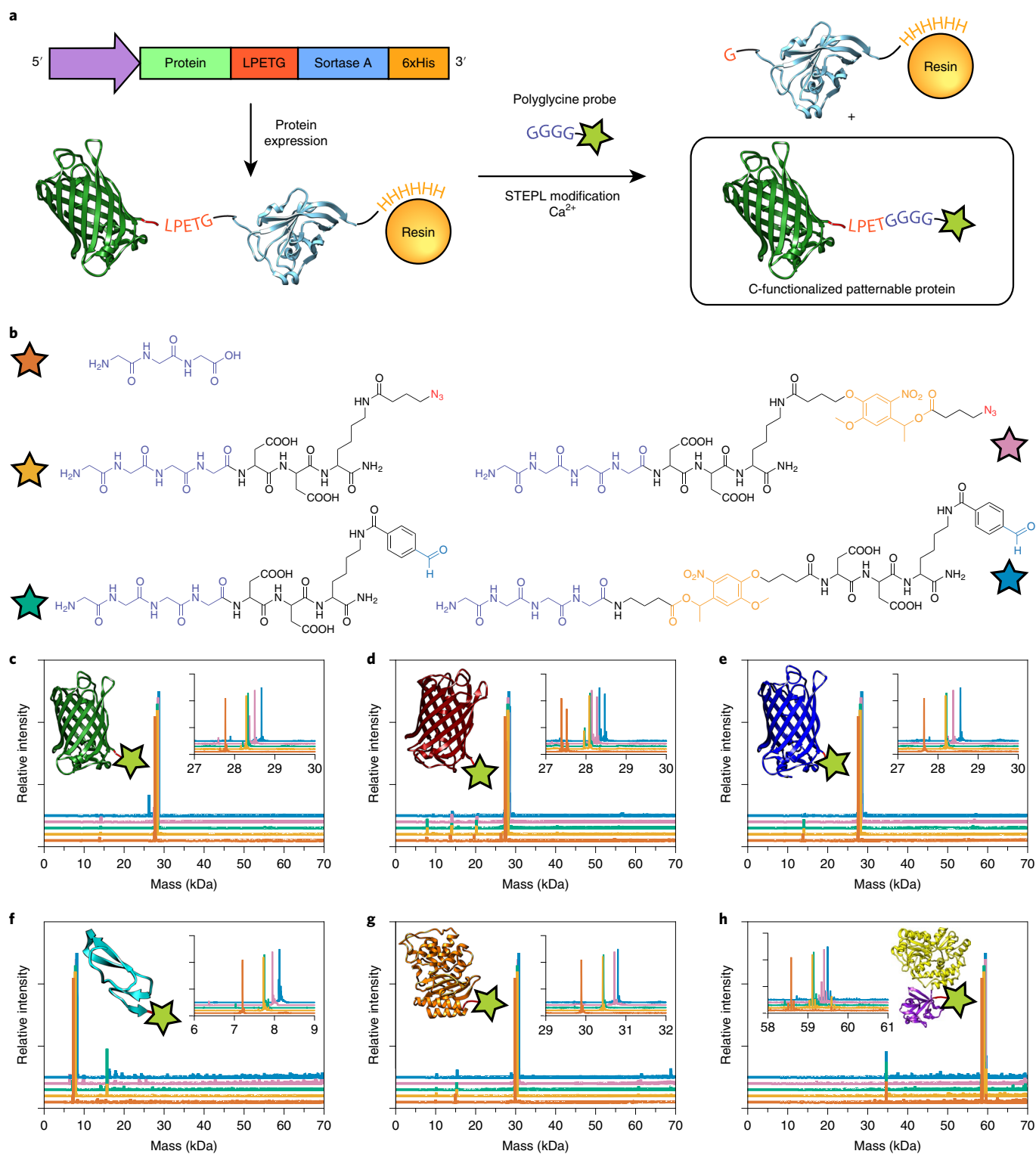


Fig. 1 | Generation of sortagged protein library for biomaterial modification. **a**, STEPL enables one-step protein biofunctionalization and purification of C-modified proteins for biomaterial decoration. Proteins appended with a genetically encoded sorting signal are expressed as a fusion with the sortase enzyme and a 6xHis tag. After chromatographic isolation on the Ni-NTA resin, intramolecular sortagging is promoted by the addition of calcium and a polyglycine probe, which catalyses peptide ligation to the protein of interest and a simultaneous displacement from the 6xHis-functionalized sortase A. The final protein functionality is defined by the polyglycine compound identity. **b**, Five distinct polyglycine probes each with different reactive functional groups that enable biomaterial decoration were synthesized and exploited for STEPL: triglycine, H-GGGGDDK(N_3)- NH_2 , H-GGGGDDK(CHO)- NH_2 , H-GGGGDDK(oNB- N_3)- NH_2 and H-GGGG-oNB-DDK(CHO)- NH_2 (denoted, respectively, with orange, tan, teal, pink and blue stars). **c-h**, Whole-protein mass spectrometry of sortagged proteins EGFP (**c**), mCherry (**d**), mCerulean (**e**), EGF (**f**), bla (**g**) and FGF (**h**) indicates a high sample purity and quantitative functionalization for all the polyglycine probes. Colours denote the probe identity as in the scheme for **b**. The double peaks in **d** indicate an incomplete N-terminal methionine excision common to mCherry expression. The spectra in **c-h** correspond to observed masses from a single purification of each species.

compound may contain non-natural functionality, which provides a route to 'sortag' a wide variety of bioorthogonal and reactive moieties site specifically onto the proteins of interest. We hypothesized that these selectively monofunctionalized species would retain a significantly higher activity than those generated through random modification, and that sortagged species would open the door to precisely regulate advanced cellular functions throughout biomaterials that have proved inaccessible via conventional strategies.

To facilitate the one-step protein biofunctionalization and purification, we implemented sortagging through the recently developed sortase-tag enhanced protein ligation (STEPL) technique³⁷ (Fig. 1a). In STEPL, the protein of interest, sorting sequence LPETG, (GGG)₅ flexible linker, sortase A and a 6xHis-Tag are fused into a single protein construct that is recombinantly expressed. The flexible (GGG)₅ linker allows intramolecular sortagging through the encoded LPETG motif and the fused sortase domain. The sortase-LPETG intermediate is displaced by the addition of calcium and a customizable probe with an N-terminal polyglycine moiety, which ligates the protein of interest to the engineered peptide and simultaneously separates it from the remaining 6xHis-functionalized sortase A. This step can be performed during immobilized metal ion affinity chromatography, in which sortase A remains bound to the nickel-nitrilotriacetic acid (Ni-NTA) column, which allows for the site-specific labelling and purification of proteins in a single step.

To highlight the versatility of sortase for protein modification and to generate a library of functional biomacromolecules for hydrogel modification, we constructed STEPL expression systems for six proteins that span three distinct classes: fluorescent (enhanced green fluorescent protein (EGFP), mCherry and mCerulean), enzymatic (β -lactamase (bla)) and growth factor (epidermal growth factor (EGF) and fibroblast growth factor (FGF)) (Supplementary Methods). As the protein functional modification by sortase is defined by the engineered peptide identity, we synthesized and exploited five distinct polyglycine probes (Fig. 1b and Supplementary Methods), each with different reactive handles (azides, aromatic aldehydes and nitrobenzyl moieties). These bioorthogonal handles enable proteins to be conjugated to materials formed by a variety of common gel formation click chemistries (such as azide/alkyne, oxime and hydrazine conjugation), as well as dictate how functionalized proteins interface with materials over time. With these six expression vectors and five sortaggable probes in hand, STEPL was utilized to generate all 30 possible protein-peptide conjugates (Supplementary Methods and Supplementary Table 1). Whole-protein mass spectrometry and gel shift assays revealed an exceptionally high protein purity and quantitative functionalization in all cases (Fig. 1c–h, Methods and Supplementary Figs. 1 and 2), which indicates the efficient generation of a diverse

collection of singly modified proteins for gel patterning. This represents the largest library of sortagged proteins created for any application to date.

Having successfully generated site-specifically modified proteins that bear the functionality required for gel decoration, we sought to compare the effects of sortagged modification versus the stochastic N-hydroxysuccinimide (NHS) ester labelling of solvent-accessible amines, the most commonly employed method to modify proteins, by using a representative protein from each class (Fig. 2a–i). EGFP activity was evaluated directly through fluorescence measurements. The activity of bla was determined through a standard colorimetric assay that involved hydrolysis of the chromogenic cephalosporin nitrocefin. EGF activity was quantified using HeLa cells that express EKAREV, a Förster resonance energy transfer (FRET) reporter for mitogen-activated protein kinase (MAPK) signalling³⁸. In all cases, azide-modified proteins sortagged with H-GGGGDDK(N₃)-NH₂ exhibited activity that was statistically indistinguishable from that of the native species. In contrast, protein bioactivity decreased significantly when azide tagging occurred through conventional NHS ester labelling that involves 2,5-dioxopyrrolidin-1-yl 4-azidobutanoate (N₃-OSu). We note that large molar excesses of the NHS-activated compound relative to the protein of interest are required for even modest levels of protein labelling (Supplementary Fig. 3), as NHS ester hydrolysis represents the dominant reaction pathway when this chemistry is performed in aqueous systems³⁹. We also note that individual proteins tolerate different amounts of random modification, as higher excesses of the NHS species were required to diminish EGFP fluorescence (a protein that has been engineered for its stable structure) than bla enzyme activity. Taken together, these experiments demonstrate that sortagging allows for the creation of modified protein conjugates with a higher purity and bioactivity than their NHS-modified counterparts.

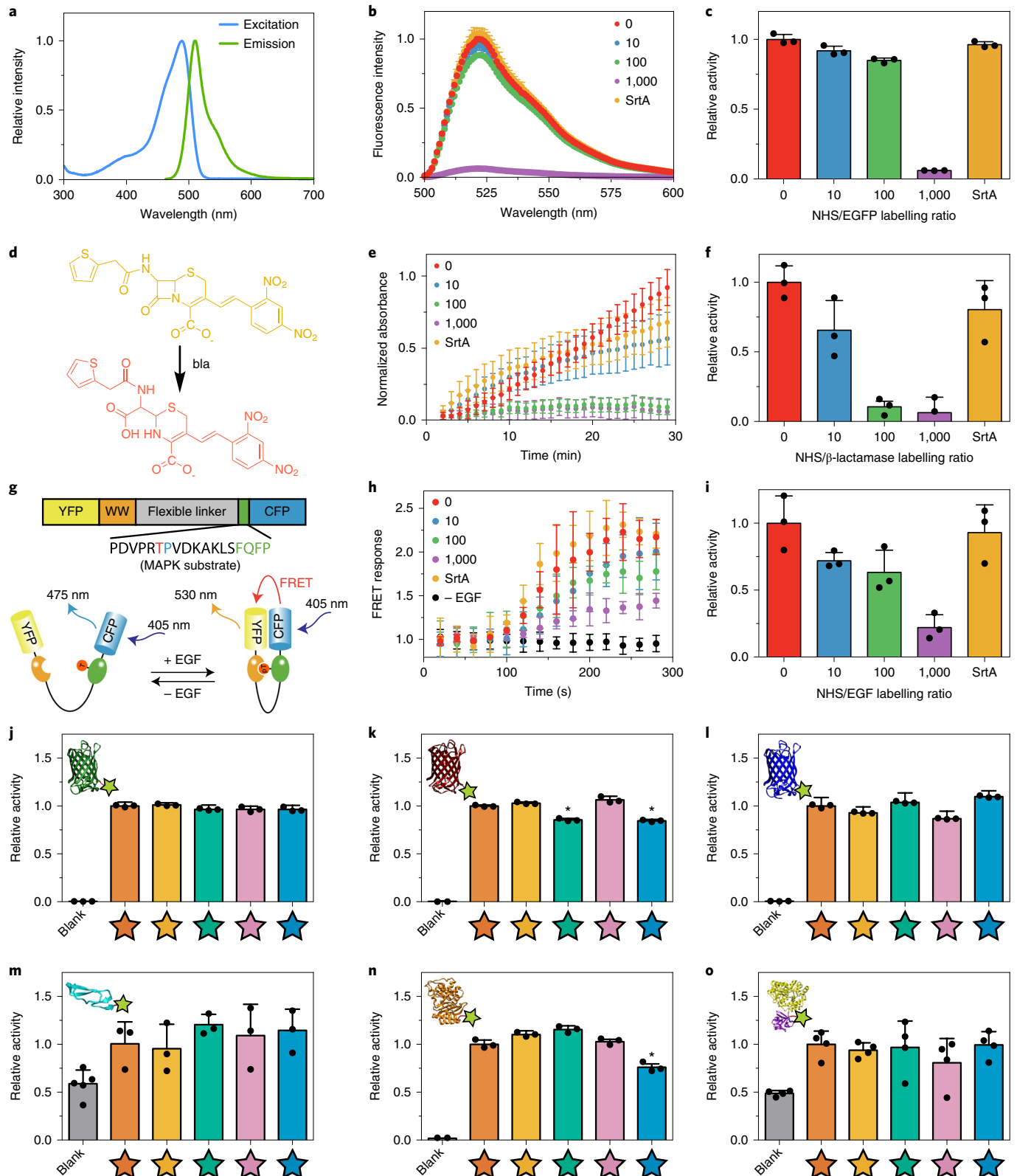
Having observed that sortagging outperformed NHS chemistry when reactive azides are introduced onto EGFP, bla and EGF, we set out to quantify the bioactivity of all 30 protein-peptide library members (Fig. 2j–o). As for EGFP, the mCherry and mCerulean activities were evaluated directly through fluorescence measurements. FGF and EGF activity were determined based on their ability to stimulate cell proliferation, quantified by increased double-stranded DNA synthesis and content. In total, the overwhelming majority (27/30) of the modified proteins exhibited bioactivity that is statistically indistinguishable from the unmodified species. Moreover, the least-active conjugate (bla-*o*NB-CHO (*o*NB, *ortho*-nitrobenzyl ester), based on the kinetically perfect bla enzyme that had previously proved highly sensitive to modification) retained 76 ± 4% of its native bioactivity. We expected the ability to singly modify functionally diverse bioactive proteins with several different

Fig. 2 | Comparing the activity of differently modified proteins. a–i. Bioactivity was compared for proteins azide-tagged by STEPL with H-GGGGDDK(N₃)-NH₂ (SrtA) or by conventional NHS labelling with varying molar excesses of N₃-OSu (0, 10, 100 and 1,000). **a**, EGFP fluorescence was used as a surrogate readout of its activity after protein modification. **b**, Fluorescence emission spectra were determined for modified EGFP ($\lambda_{\text{excitation}} = 470$ nm). **c**, Increasing NHS modification led to a decrease in EGFP emission ($\lambda_{\text{excitation}} = 470$ nm, $\lambda_{\text{emission}} = 530$ nm), whereas sortagged EGFP retained a native-like fluorescence. **d**, Bla activity was determined by its ability to degrade a chromogenic nitrocefin substrate, which changes from yellow to red on β -lactam cleavage. **e**, Time-course spectrophotometric analyses ($\lambda_{\text{abs}} = 386$ nm) indicate nitrocefin degradation for NHS-modified and sortagged bla. **f**, Sortagged and unmodified bla exhibited statistically indistinguishable levels of bioactivity, as indicated by similar values for k_{cat} . Bla displayed a high sensitivity to NHS labelling, probably due to the presence of a critical lysine residue in its active pocket. **g**, The activity of EGF was quantitatively determined with a HeLa cell line that expressed the EKAREV FRET reporter for MAPK activation. Functional EGF catalyses the phosphorylation of a MAPK substrate, which results in an intramolecular association that co-localizes a yellow fluorescent protein (YFP) and cyan fluorescent protein (CFP) FRET pair. **h**, The YFP/CFP FRET ratios after growth factor stimulation were determined for modified EGF. **i**, Increased NHS labelling of EGF yielded a decreased bioactivity, as determined by the initial rate of change in the FRET response, whereas the sortagged growth factor exhibited native levels of activity. **j–o**, Relative bioactivity of proteins EGFP (**j**), mCherry (**k**), mCerulean (**l**), EGF (**m**), bla (**n**) and FGF (**o**) sortagged with triglycine, H-GGGGDDK(N₃)-NH₂, H-GGGGDDK(CHO)-NH₂, H-GGGGDDK(*o*NB-N₃)-NH₂ and H-GGGG-*o*NB-DDK(CHO)-NH₂ (denoted, respectively, with orange, tan, teal, pink and blue stars). Asterisks denote conjugates with a statistically significant reduction in bioactivity ($P < 0.05$), as compared to the unmodified species (unpaired two-tailed t -test, $P = 1.3 \times 10^{-4}$ for mCherry-CHO, $P = 3.5 \times 10^{-4}$ for mCherry-*o*NB-CHO, $P = 3.2 \times 10^{-3}$ for bla-*o*NB-CHO). Error bars correspond to the s.d. about the mean for biological replicate experiments ($n = 3$ for studies that involved fluorescent proteins, bla and EGF; $n = 4$ for FGF).

reactive handles, each of which influences how they form the basis of and interact with materials, to hugely enable a variety of biological applications. Additionally, the relative ease and lack of specialized equipment required for protein expression and/or purification, coupled with the commercial availability of sortagable peptides

that contain functional handles (which include azides, alkynes, (meth)acrylates, thiols, aldehydes, maleimides and allyl sulfides), render these strategies practically accessible to non-specialists.

After verifying that sortagged proteins retained the native bio-activity, we sought to demonstrate their controlled incorporation



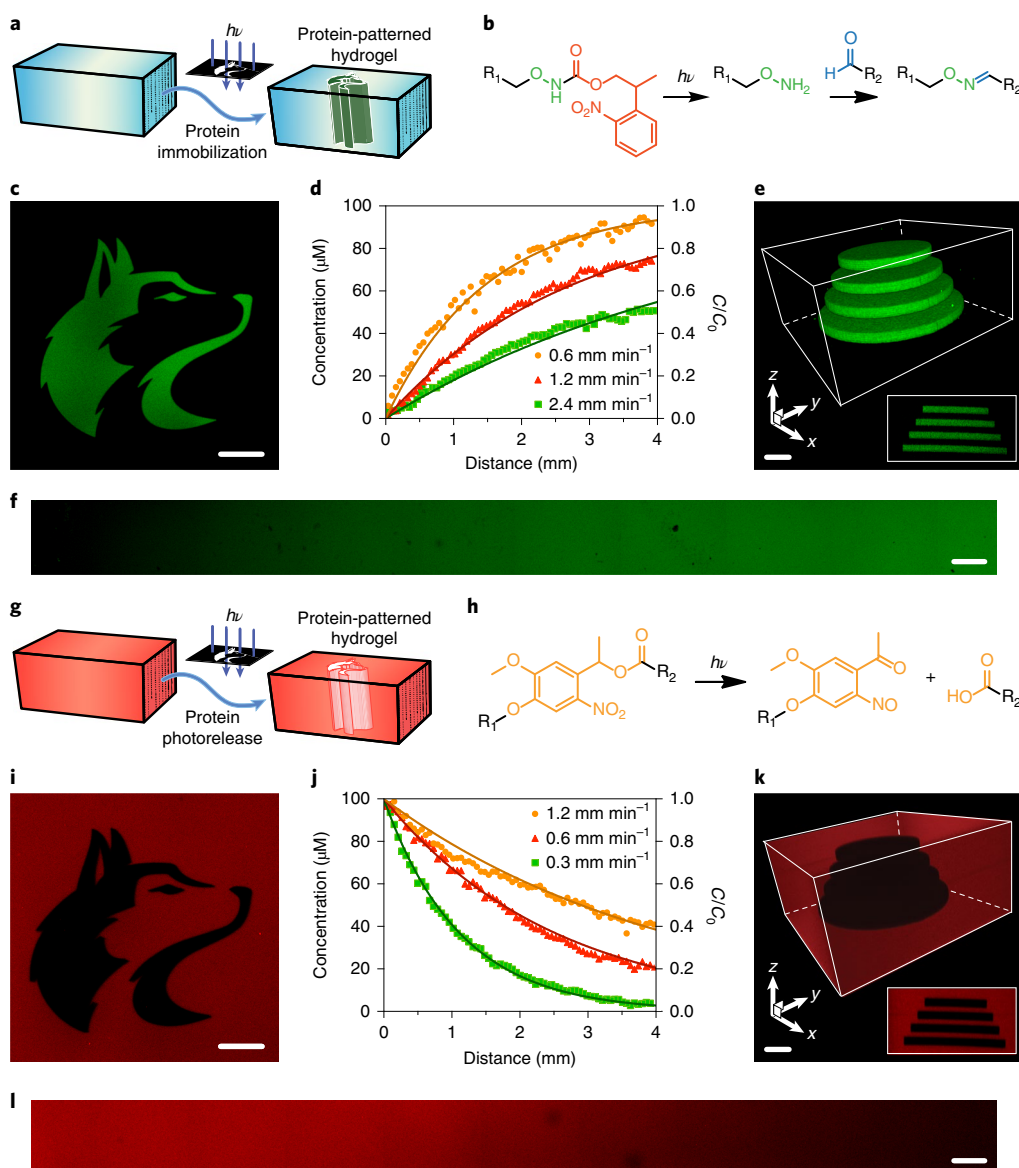


Fig. 3 | Photopatterned alteration of hydrogel biomaterials with sortagged proteins. **a–f**, Photopatterned immobilization of sortagged proteins within gels. **a**, Proteins modified site specifically with aromatic aldehydes are immobilized within SPAAC-based gels through photomediated oxime ligation. **b**, NPPOC-caged alkoxyamines distributed uniformly throughout the gels (R_1) undergo irreversible β -elimination on mild ultraviolet exposure ($\lambda = 365$ nm or 740 nm). The deprotected alkoxyamines react with aldehyde-tagged proteins (R_2) to form stable oxime linkages. **c**, Mask-based photolithography ($\lambda = 365$ nm) was used to immobilize discrete patterns of EGFP-CHO throughout the gel thickness. **d,f**, By exposing gel surfaces to linear gradients of light exposure (created by covering samples with an opaque photomask that moves at rates of 0.6, 1.2 and 2.4 mm min⁻¹, 10 mW cm⁻² and $\lambda = 365$ nm), exponential protein gradients were generated in a dose-dependent manner. C_0 represents the highest possible protein concentration that can be immobilized (determined based on the 100 μ M caged alkoxyamine included during gel formulation). **e**, Full 3D control over protein tethering within the gels is achieved through multiphoton laser-scanning lithographic patterning ($\lambda = 740$ nm). **g–l**, The photopatterned release of sortagged proteins from gels. **g**, Site-specifically modified proteins are released from SPAAC-based gels through oNB photocleavage. **h**, oNB moieties linking the sortagged proteins (R_1) and the hydrogel (R_2) undergo a rapid photocleavage on a mild UV exposure ($\lambda = 365$ nm or 740 nm). **i**, Mask-based photolithography ($\lambda = 365$ nm) was used to dictate discrete patterns of protein release from gels uniformly functionalized with mCherry-oNB-N₃. **j,l**, By exposing gel surfaces to linear gradients of light exposure (created by covering samples with an opaque photomask moving at rates of 0.3, 0.6 and 1.2 mm min⁻¹, 10 mW cm⁻² and $\lambda = 365$ nm), exponential protein gradients were generated in a dose-dependent manner. C_0 corresponds to the initial mCherry concentration included during the gel formulation (100 μ M). **k**, Full 3D control over protein release within the gels is achieved through multiphoton laser-scanning lithographic patterning ($\lambda = 740$ nm). Immobilized protein concentrations in **d** and **j** are determined through fluorescence correlation. The solid curves in **d** and **j** are predicted by known NPPOC/oNB photocleavage kinetics. The images in **c**, **e**, **f**, **i**, **k** and **l** correspond to representative individual gels imaged by fluorescence confocal microscopy. The data in **d** and **j** are derived from experiments that involved single gels for each gradient light condition. The inset in **e** corresponds to a maximum-intensity y projection, whereas that in **k** corresponds to a minimum-intensity y projection. Scale bars, 100 μ m.

within biomaterials. Exploiting strategies previously introduced by our laboratory²⁷, we utilized model hydrogels formed through strain-promoted azide-alkyne cycloaddition (SPAAC) between a

four-arm poly(ethylene glycol) (PEG) tetrabicyclononyne and a linear PEG diazide (Supplementary Methods). Reaction kinetics and bioorthogonality permit the encapsulation of live cells with a high

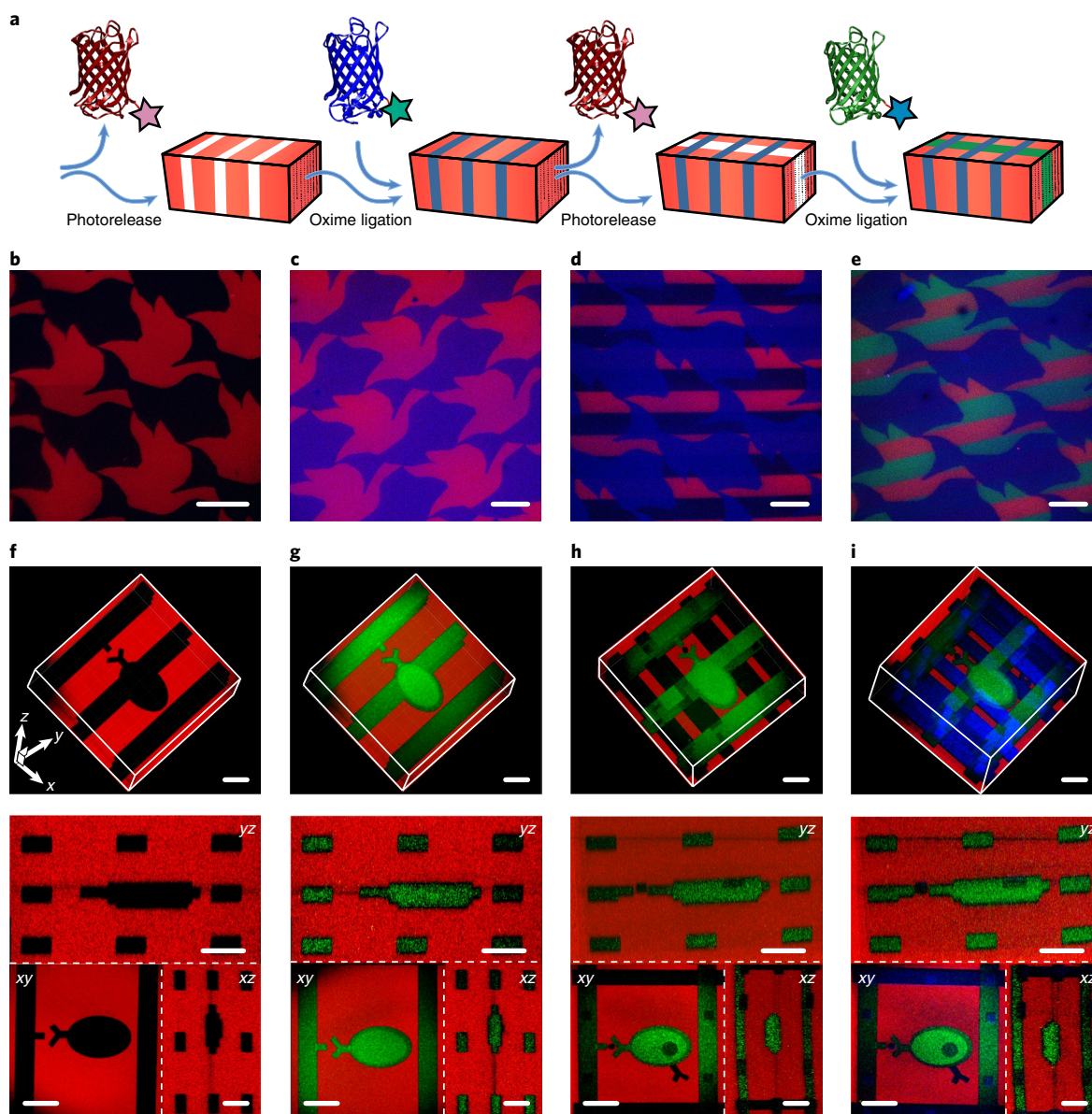


Fig. 4 | 4D photoevolution of hydrogel biomaterials patterned with multiple sortagged proteins. **a**, Protein photorelease can be performed in concert with the photomediated ligation of an aldehyde-tagged protein to create complex interconnected biochemical patterns. Iteration of this process enables the 4D evolution of protein patterns within the gels. **b–e**, Masked-based photolithographic techniques ($\lambda = 365$ nm) were utilized to control the sequential protein patterning in defined shapes that extend throughout the gel thickness. **b,c**, After the directed exposure of gels uniformly functionalized with mCherry-oNB-N₃ (red) (**b**), mCherry is released while uncaging sites for subsequent mCerulean-CHO (blue) immobilization by oxime ligation (**c**). **d**, A second round of directed light exposure released additional mCherry and left the mCerulean patterns intact. **e**, EGFP-oNB-CHO (green) is immobilized in the uncaged alkoxyamine sites to create a trifunctional protein pattern. **f–i**, The evolution of trifunctional protein patterns was controlled in 3D space through multiphoton laser-scanning lithography ($\lambda = 740$ nm). The rows in **f–i** correspond to 3D renderings of the photoevolved materials, in which red (mCherry) channels represent the minimum intensity projections and green (EGFP) and blue (mCerulean) are the maximum intensity projections (first row), as well as the yz (second row) and xy and xz (third row) planar slices. The photorelease of mCherry-oNB-N₃ (**f**) is followed by protein backfilling with EGFP-oNB-CHO (**g**). Further treatment with pulsed laser light released both EGFP-oNB-CHO and mCherry-oNB-N₃ within user-specified gel subvolumes (**h**) to create anchoring sites for mCerulean-CHO immobilization (**i**). The images in **b–i** were generated using fluorescence confocal microscopy on a single gel throughout sequential patterning. Scale bars, 100 μm.

viability, and the bioinert PEG provides a non-fouling ‘blank slate’ for the subsequent decoration with proteins. The optical clarity of these materials renders them useful for photochemical modification with biomolecules, as well as for microscopy-based assays of the fate of the encapsulated cell.

A cytocompatible photomediated oxime ligation^{27,40} was exploited to immobilize site-specifically modified proteins within

hydrogels that contained a 2-(2-nitrophenyl)propyloxycarbonyl (NPPOC)-photocaged alkoxyamine with spatiotemporal control (Fig. 3a,b). On mild near-ultraviolet (UV) irradiation ($\lambda = 365$ nm), NPPOC is cleaved, which liberates the reactive alkoxyamine and permits a localized condensation with gel-swollen aromatic aldehyde-modified proteins to form a stable oxime linkage. The removal of unbound proteins by diffusion yields patterned gel substrates

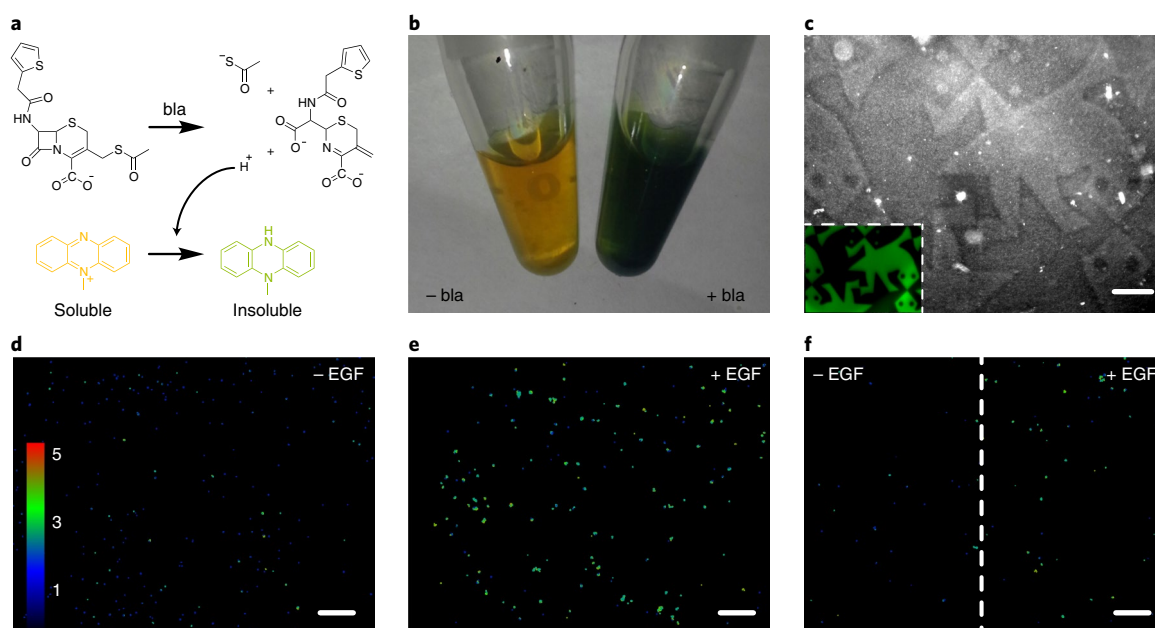


Fig. 5 | Spatial patterning of gels with bioactive site-specifically modified enzymes and growth factors. **a**, Thioacetate cefalotin is hydrolysed enzymatically by bla, which eliminates protons and thiolate ions that reduce a water-soluble yellow phenazine into a green water-insoluble precipitate. **b**, In-solution treatment of thioacetate cefalotin (5 mM) and phenazine methosulfate (6.5 mM) with bla (30 μ M) yields a distinct colour change and precipitate formation. **c**, Gels that contained photopatterned regions of immobilized bla were visualized by phase contrast microscopy on treatment with thioacetate cefalotin and phenazine methosulfate. Insoluble precipitation was confined to bla-modified gel subvolumes. Inset corresponds to an EGFP-modified gel with the same tessellated protein pattern. **d**, HeLa cells encapsulated in gels and expressing the EKAREV FRET reporter for MAPK signalling exhibit basal signalling. **e**, Average intracellular MAPK activation increases about twofold when gels are uniformly functionalized with EGF (12.5 nM). **f**, A high MAPK activation persisted in EGF-patterned gel regions, whereas no upregulation in MAPK levels was observed in unfunctionalized regions. The images in **d–f** represent colour-coded FRET responses normalized to basal MAPK activation, obtained from confocal z slices. All the experiments were conducted in triplicate ($n=3$) with similar results. Scale bars, 250 μ m.

defined by user-selected light-exposure locations and parameters. Gel patterning was performed with EGFP sortagged with H-GGGGDDK(CHO)-NH₂ (EGFP-CHO), whereby the immobilized protein fluorescence permitted visualization and quantification. Traditional photolithographic techniques were utilized to control the patterning of the mask-defined shapes throughout the gel thickness (Fig. 3c) and to generate continuous gradients that followed a dose-dependent response predicted by NPPOC photocleavage kinetics (Fig. 3d,f and Supplementary Fig. 4). EGFP-CHO was immobilized within the hydrogels with an excellent 3D control through multiphoton laser-scanning lithography, whereby programmed laser rastering within the gel material dictated the protein tethering location and concentration (Fig. 3e and Supplementary Fig. 5). These experiments represent the first demonstration of the 3D patterned covalent immobilization of a site-specifically modified protein within a material.

After having demonstrated the ability to immobilize sortagged proteins within biomaterials with excellent 3D control, we shifted our efforts towards the patterned photorelease of such species from gels (Fig. 3g). For this, we exploited an *ortho*-nitrobenzyl ester (oNB) moiety^{22,41} that undergoes rapid photocleavage in response to cytocompatible near-UV light ($\lambda=365$ nm) (Fig. 3h). mCherry sortagged with H-GGGGDDK(oNB-N₃)-NH₂ (mCherry-oNB-N₃) was tethered uniformly throughout the materials during the SPAAC-based gelation. After a directed light exposure, released protein was diffused from the gel prior to sample imaging and quantification through fluorescent confocal microscopy. Mask-based photolithographic techniques were again exploited to control the mCherry-oNB-N₃ removal and concentration throughout the full gel thickness in a predictable and dose-dependent manner

(Fig. 3i,j,l and Supplementary Figs. 6 and 7). Multiphoton lithography afforded an excellent 3D patterning at user-specified regions within the gels (Fig. 3k and Supplementary Fig. 8). In addition to controlling the location of the immobilized proteins that persist within a gel, the fully defined and homogeneous protein population photoreleased from the material may have significant implications for controlled drug delivery.

Sortase's versatility in introducing diverse functional handles onto different proteins of interest enables protein-patterned materials of unprecedented complexity to be photoevolved in 4D. To demonstrate the dynamic material patterning, we selected three differentially modified and spectrally separated fluorescent proteins from our library of sortagged species. Gels that contained the NPPOC-caged alkoxyamine were uniformly functionalized with mCherry-oNB-N₃. On a directed light exposure, mCherry photorelease was performed in concert with the photomediated ligation of an aldehyde-tagged protein (either mCerulean-CHO or EGFP-oNB-CHO) to create interconnected biochemical patterns. The photorelease/oxime ligation sequence was repeated, which enabled a third protein (either EGFP-oNB-CHO or mCerulean-CHO) to be immobilized (Fig. 4a). This approach was utilized to create an Escher-inspired tessellation of fish and bird shapes through masked lithography (Fig. 4b–e and Supplementary Fig. 9), as well as a 3D schematic depiction of a cell binding to an ECM-presented ligand via multiphoton patterning (Fig. 4f–i, Supplementary Fig. 10 and Supplementary Videos 1 and 2). Collectively, these data demonstrate a dynamic control over multiple factors in time and space with unmatched precision, as well as the 4D regulation of site-specifically modified proteins within materials.

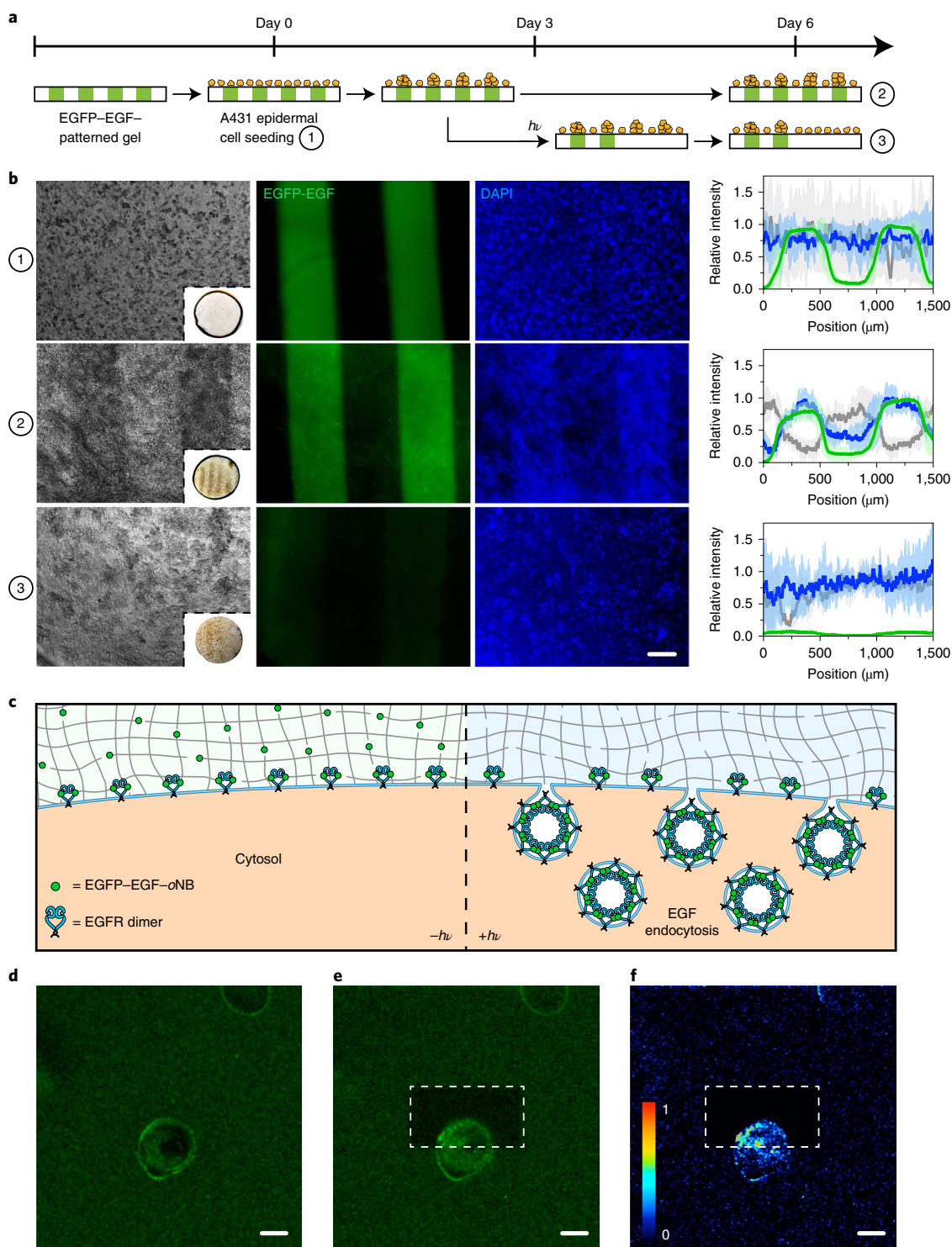


Fig. 6 | Modulating cell fate with a photoreleasable sortagged fluorophore growth factor chimeric protein. **a**, The patterned population-level control of A431 cell proliferation is achieved through stimulation with gel-immobilized EGFP-EGF-oNB-N₃ in a 2D culture. Protein photoremoval promotes a dynamic cell redistribution. The key analytical timepoints are noted on the experimental timeline with circled numbers. **b**, Brightfield (left) and fluorescent images (centre columns) highlight the cell response (nuclei in blue) to patterned EGFP-EGF-oNB-N₃ (green) at various experimental endpoints. Relative intensity profiles (right column) are given for EGFP (green), nuclei (blue) and optical transmission (grey) across the gels perpendicular to the photopatterned lines, with average values (dark lines) and s.d. (light error bars) that correspond to data from three biological replicates ($n=3$). The brightfield insets depict full hydrogel (~0.5 cm in diameter). The images and analysis in condition three correspond to the gel half whose protein was photoreleased on day 3. DAPI, 4',6-diamidino-2-phenylindole. **c**, Encapsulated cells bind but cannot internalize hydrogel-tethered EGFP-EGF-oNB-N₃ (left). Photoliberation of the soluble protein promotes canonical EGFR activation and the associated membrane endocytosis (right). **d,e**, EGFP-EGF protein release is confined to gel subvolumes that bisect a single A431 cell in 3D culture. The endosome formation is visible in <5 min and is concentrated in the regions of light exposure. Fluorescent images correspond to timepoints immediately preceding (**d**) and 5 min after (**e**) the protein photorelease within a single gel. **f**, The difference calculations between images pre- and postrelease highlight the local EGFP-EGF internalization. Scale bars, 200 μm (**b**) and 10 μm (**d-f**).

Encouraged that mCherry, mCerulean and EGFP each retained their fluorescence and spatial patterning for several weeks after hydrogel tethering, we sought to determine whether we could confine enzymatic activity to user-specified gel subvolumes. Utilizing bla-*oNB-N₃*, we functionalized and patterned gels through mask-based protein photoremoval. Protein-patterned gels were treated with 7-thiophenylacetamido-3-thioacetoxymethyl-3-cephem-4-carboxylate⁴² (thioacetate cefalotin (Supplementary Methods)), a thiocephalosporin that eliminates a proton and a thiolate ion after β -lactam enzymatic hydrolysis to reduce the water-soluble yellow phenazine into a green water-insoluble precipitate (Fig. 5a,b). Phase contrast microscopy indicated changes in the localized refractive index that correspond to an enzyme-induced precipitation confined to the bla-modified regions within the gel (Fig. 5c and Supplementary Fig. 11). This is a successful example of confining enzymatic activity to photopatterned locations within a material, a task enabled by site-specific modification and that is likely to prove useful in enzymatically regulating critical ECM parameters.

Having demonstrated that sortagged enzymes remain active when photopatterned within gels and that gel formation and modification chemistries are cytocompatible (Supplementary Fig. 12), we tested the ability of these techniques to direct local cell function using immobilized growth factors. HeLa cells transfected with the EKAREV FRET reporter for MAPK activation³⁸ were encapsulated in materials uniformly functionalized with EGF-*oNB-N₃*. After a complete bulk protein photorelease, the cells displayed basal levels of MAPK activation; those in which EGF remained immobilized elicited significantly higher (about twofold) intracellular signalling (Fig. 6d–e). The extent of the FRET responses for cells in 3D was consistent with 2D studies that involved soluble EGF (Supplementary Figs 13 and Supplementary Video 3) and is not directly affected by the light treatments used for gel photomodulation (Supplementary Fig. 14). Taking advantage of the spatial control afforded by protein photorelease, gels with a patterned EGF were created through masked exposure; MAPK activation remained high in gel subvolumes still functionalized with EGF, but returned to basal levels in those in which the protein had been photoreleased. As MAPK signalling plays a key role in regulating cell proliferation, migration and differentiation, its patterned activation represents a powerful step towards regulating advanced cell fates with a spatiotemporal control.

An added benefit of using STEPL to modify proteins for material decoration is its compatibility with many standard protein engineering strategies. Although the photoremovable EGF proved successful in spatially regulating MAPK activation in 3D gels, its location cannot be directly visualized during experimentation. To address this limitation, we constructed an expression vector for an EGFP-EGF fusion and performed STEPL using H-GGGGDDK(*oNB-N₃*)-NH₂ to generate EGFP-EGF-*oNB-N₃* (Supplementary Methods and Supplementary Fig. 15). Taking advantage of its fluorescence, bioactivity, tetherability and photoreleasability, we first used this tetrafunctional protein to pattern proliferation through dynamic EGF stimulation (Fig. 6a,b). Epidermal A431 cells were seeded on hydrogels that contained interspaced lines of EGFP-EGF-*oNB-N₃*. The immobilized EGFP-EGF remained effective in driving proliferation, with cell patterning visibly evident by day 3 (Supplementary Fig. 16); functionalized regions yielded an about twofold increase in cell densities relative to those that lacked EGF by day 6. Control experiments with the patterned EGFP exhibited homogeneous surface coverage with no significant difference in cell localization based on the underlying fluorescent protein pattern at any observed time point (Supplementary Fig. 17). To assay the effects of dynamically patterned EGF stimulation on cell function, a parallel experiment was constructed in which the EGFP-EGF was photoreleased from one-half of each individual line-patterned gel three days into the culture. Although the persistently functionalized gel portions

exhibited the expected patterning in cell density, a uniform surface coverage was observed across the photoreleased gel portions where, presumably, cells had redistributed through migration to eliminate any previously patterned heterogeneity (Supplementary Fig. 18). 3D experiments that involved encapsulated HeLa cells yielded similar results, in which spheroid growth was enhanced with persistently patterned EGFP-EGF (Supplementary Figs. 19–21). Through the reversibly controlled presentation of bioactive growth factors, we demonstrate a newfound ability to modulate local proliferation/migration of cells in 2D and 3D.

Armed with the EGFP-EGF-*oNB-N₃* tetrafunctional chimera, we sought to demonstrate that photoreleased proteins could influence dynamic biological fate with resolutions previously inaccessible to biomaterial-based approaches. EGF binds the cell surface protein epidermal growth factor receptor (EGFR) to yield an activated transmembrane protein that undergoes homodimerization. Canonical EGFR activation is coupled with membrane endocytosis, receptor trafficking and downstream signal transduction. Although matrix-bound EGF binds EGFR, growth factor tethering inhibits ligand-receptor internalization, endocytotic trafficking and canonical signalling^{43,44}. We hypothesized that the photoliberation of soluble EGFP-EGF could be used to 'turn on' canonical EGFR activation locally within the culture and that downstream endosome formation could be visualized with fluorescent microscopy (Fig. 6c and Supplementary Fig. 22). To test this hypothesis, A431 cells were encapsulated in gels modified with EGFP-EGF-*oNB-N₃*. Confocal imaging revealed a fluorescent halo that initially outlined each cell, which indicates ligand-receptor binding and the presence of concentrated membrane-bound EGFP-EGF (Fig. 6d). Multiphoton laser-scanning lithography was used to selectively release the EGFP-EGF protein on one side of an individual encapsulated cell, which triggered the EGFP-EGF untethering and local endocytic vesicle formation, visible in <5 minutes and concentrated in the regions of light exposure (Fig. 6e,f). Cells within the same imaging window (~50 μ m away) were unaffected by the photoreleased EGF, which further indicates that activation could be specified with single micrometre-scale precision. Control studies that involved photoreleasable EGFP did not yield endocytosis (Supplementary Fig. 23). This importantly demonstrates the utility that dynamic materials can have in governing 3D biological fate with single-cell and/or subcellular resolution.

The results described here introduce and highlight the sortase-mediated transpeptidation as a uniquely powerful strategy to create a diverse library of homogeneous, singly modified proteins with non-natural functionality. Sortagged proteins can be efficiently expressed and purified by STEPL, and exhibit near-native bioactivity while affording the ability to decorate biomaterials in a user-dictated manner. By specifying the reactive handle identity, functional proteins can be reversibly immobilized within hydrogels with excellent spatiotemporal resolution through a variety of bioorthogonal photochemical reactions. Such a patterned control over niche biochemical properties with homogeneous proteins permits the unprecedented regulation of complex biological functions and cellular pathways. We expect that this approach will prove useful in probing the effects of ECM-presented cues on single-cell fate and in the design of materials for tissue engineering, which potentially opens the door to multilineage patterning of 3D stem cell differentiation.

Online content

Any methods, additional references, Nature Research reporting summaries, source data, statements of code and data availability and associated accession codes are available at <https://doi.org/10.1038/s41563-019-0367-7>.

Received: 23 August 2017; Accepted: 9 April 2019;
Published online: 20 May 2019

References

- Lutolf, M. P., Gilbert, P. M. & Blau, H. M. Designing materials to direct stem-cell fate. *Nature* **462**, 433–441 (2009).
- Tibbitt, M. W. & Anseth, K. S. Dynamic microenvironments: the fourth dimension. *Sci. Transl. Med.* **4**, 160ps24 (2012).
- Baker, B. M. & Chen, C. S. Deconstructing the third dimension—how 3D culture microenvironments alter cellular cues. *J. Cell Sci.* **125**, 3015–3024 (2012).
- DeForest, C. A. & Anseth, K. S. Advances in bioactive hydrogels to probe and direct cell fate. *Annu. Rev. Chem. Biomol. Eng.* **3**, 421–444 (2012).
- Burdick, J. A. & Murphy, W. L. Moving from static to dynamic complexity in hydrogel design. *Nat. Commun.* **3**, 1269 (2012).
- Langer, R. & Vacanti, J. P. Tissue engineering. *Science* **260**, 920–926 (1993).
- Lee, K. Y. & Mooney, D. J. Hydrogels for tissue engineering. *Chem. Rev.* **101**, 1869–1879 (2001).
- Langer, R. & Tirrell, D. A. Designing materials for biology and medicine. *Nature* **428**, 487–492 (2004).
- Cushing, M. C. & Anseth, K. S. Hydrogel cell cultures. *Science* **316**, 1133–1134 (2007).
- Tibbitt, M. W. & Anseth, K. S. Hydrogels as extracellular matrix mimics for 3D cell culture. *Biotechnol. Bioeng.* **103**, 655–663 (2009).
- Seliktar, D. Designing cell-compatible hydrogels for biomedical applications. *Science* **336**, 1124–1128 (2012).
- Lutolf, M. P. & Hubbell, J. A. Synthetic biomaterials as instructive extracellular microenvironments for morphogenesis in tissue engineering. *Nat. Biotechnol.* **23**, 47–55 (2005).
- Zhang, Y. S., & Khademhosseini, A. Advances in engineering hydrogels. *Science* **356**, eaaf362 (2017).
- Tam, R. Y., Smith, L. J. & Shoichet, M. S. Engineering cellular microenvironments with photo- and enzymatically responsive hydrogels: toward biomimetic 3D cell culture models. *Acc. Chem. Res.* **50**, 703–713 (2017).
- Caliari, S. R. & Burdick, J. A. A practical guide to hydrogels for cell culture. *Nat. Methods* **13**, 405–414 (2016).
- Rosales, A. M. & Anseth, K. S. The design of reversible hydrogels to capture extracellular matrix dynamics. *Nat. Rev. Mater.* **1**, 15012 (2016).
- Ruskowitz, E. R. & DeForest, C. A. Photoresponsive biomaterials for targeted drug delivery and 4D cell culture. *Nat. Rev. Mater.* **3**, 17087 (2018).
- Luo, Y. & Shoichet, M. S. A photolabile hydrogel for guided three-dimensional cell growth and migration. *Nat. Mater.* **3**, 249–253 (2004).
- Hahn, M. S., Miller, J. S. & West, J. L. Three-dimensional biochemical and biomechanical patterning of hydrogels for guiding cell behavior. *Adv. Mater.* **18**, 2679–2684 (2006).
- DeForest, C. A., Polizzotti, B. D. & Anseth, K. S. Sequential click reactions for synthesizing and patterning three-dimensional cell microenvironments. *Nat. Mater.* **8**, 659–664 (2009).
- DeForest, C. A., Sims, E. A. & Anseth, K. S. Peptide-functionalized click hydrogels with independently tunable mechanics and chemical functionality for 3D cell culture. *Chem. Mater.* **22**, 4783–4790 (2010).
- DeForest, C. A. & Anseth, K. S. Cytocompatible click-based hydrogels with dynamically tunable properties through orthogonal photoconjugation and photocleavage reactions. *Nat. Chem.* **3**, 925–931 (2011).
- DeForest, C. A. & Anseth, K. S. Photoreversible patterning of biomolecules within click-based hydrogels. *Angew. Chem. Int. Ed.* **51**, 1816–1819 (2012).
- Wylie, R. G. et al. Spatially controlled simultaneous patterning of multiple growth factors in three-dimensional hydrogels. *Nat. Mater.* **10**, 799–806 (2011).
- Mosiewicz, K. A. et al. In situ cell manipulation through enzymatic hydrogel photopatterning. *Nat. Mater.* **12**, 1071–1077 (2013).
- Griffin, D. R. et al. Hybrid photopatterned enzymatic reaction (HyPER) for in situ cell manipulation. *ChemBioChem* **15**, 233–242 (2014).
- DeForest, C. A. & Tirrell, D. A. A photoreversible protein-patterning approach for guiding stem cell fate in three-dimensional gels. *Nat. Mater.* **14**, 523–531 (2015).
- Fisher, S. A., Baker, A. E. G. & Shoichet, M. S. Designing peptide and protein modified hydrogels: selecting the optimal conjugation strategy. *J. Am. Chem. Soc.* **139**, 7416–7427 (2017).
- Baslé, E., Joubert, N. & Pucheault, M. Protein chemical modification on endogenous amino acids. *Chem. Biol.* **17**, 213–227 (2010).
- Rabuka, D. Chemoenzymatic methods for site-specific protein modification. *Curr. Opin. Chem. Biol.* **14**, 790–796 (2010).
- Rabuka, D., Rush, J. S., deHart, G. W., Wu, P. & Bertozzi, C. R. Site-specific chemical protein conjugation using genetically encoded aldehyde tags. *Nat. Protoc.* **7**, 1052–1067 (2012).
- Kulkarni, C., Kinzer-Ursem, T. L. & Tirrell, D. A. Selective functionalization of the protein N terminus with N-myristoyl transferase for bioconjugation in cell lysate. *ChemBioChem* **14**, 1958–1962 (2013).
- Chen, I., Howarth, M., Lin, W. & Ting, A. Y. Site-specific labeling of cell surface proteins with biophysical probes using biotin ligase. *Nat. Methods* **2**, 99–104 (2005).
- Guimaraes, C. P. et al. Site-specific C-terminal and internal loop labeling of proteins using sortase-mediated reactions. *Nat. Protoc.* **8**, 1787–1799 (2013).
- Mao, H., Hart, S. A., Schink, A. & Pollok, B. A. Sortase-mediated protein ligation: a new method for protein engineering. *J. Am. Chem. Soc.* **126**, 2670–2671 (2004).
- Mazmanian, S. K., Liu, G., Hung, T. T. & Schneewind, O. *Staphylococcus aureus* sortase, an enzyme that anchors surface proteins to the cell wall. *Science* **285**, 760–763 (1999).
- Warden-Rothman, R., Caturegli, I., Popik, V. & Tsourkas, A. Sortase-tag expressed protein ligation: combining protein purification and site-specific bioconjugation into a single step. *Anal. Chem.* **85**, 11090–11097 (2013).
- Komatsu, N. et al. Development of an optimized backbone of FRET biosensors for kinases and GTPases. *Mol. Biol. Cell* **22**, 4647–4656 (2011).
- Hermanson, G. T. *Bioconjugate Techniques* (Academic, Cambridge, 2013).
- Farahani, P. E., Adelmund, S. M., Shadish, J. A. & DeForest, C. A. Photomediated oxime ligation as a bioorthogonal tool for spatiotemporally-controlled hydrogel formation and modification. *J. Mater. Chem. B* **5**, 4435–4442 (2017).
- Kloxin, A. M., Kasko, A. M., Salinas, C. N. & Anseth, K. S. Photodegradable hydrogels for dynamic tuning of physical and chemical properties. *Science* **324**, 59–63 (2009).
- Bieniarz, C., Young, D. F. & Cornwell, M. J. Chromogenic redox assay for β -lactamases yielding water-insoluble products. I. Kinetic behavior and redox chemistry. *Anal. Biochem.* **207**, 321–328 (1992).
- Kuhl, P. R. & Griffith-Cima, L. G. Tethered epidermal growth factor as a paradigm for growth factor-induced stimulation from the solid phase. *Nat. Med.* **2**, 1022–1027 (1996).
- Fan, V. H. et al. Tethered epidermal growth factor provides a survival advantage to mesenchymal stem cells. *Stem Cells* **25**, 1241–1251 (2007).

Acknowledgements

The authors recognize and thank R. Seifert and D. Hailey of the University of Washington Garvey Imaging Center for their ongoing support and advice, F. Watt and T. Hiratsuka (King's College London) for helpful discussion on visualizing the MAPK activation, M. Matsuda (Kyoto University) for a gift of the HeLa cells transfected with the EKAREV FRET sensor, as well as R. Warden-Rothman and A. Tsourkis (University of Pennsylvania) for providing the pSTEPL plasmid³⁷. The authors thank B. Badeau for assistance in synthesizing N₃-oNB-OSu, S. Adelmund for providing BCN-OSu and A. Im for help with the protein purification optimization. We acknowledge support from S. Edgar at the UW Mass Spectrometry Center as well as that from the NIH and N. Peters at the UW W. M. Keck Microscopy Center (S10 OD016240). This work was supported by a University of Washington Faculty Startup Grant (C.A.D.), a Jaquette L. Tietze Young Scientist Research Award (C.A.D.) and a CAREER Award (DMR 1652141, C.A.D.) from the National Science Foundation.

Author contributions

For this manuscript, J.A.S. and C.A.D. conceived and designed the experiments; J.A.S. and G.M.B. performed the experiments; J.A.S. and C.A.D. analysed the data and prepared the figures; J.A.S. and C.A.D. wrote the paper.

Competing interests

The authors declare no competing interests.

Additional information

Supplementary information is available for this paper at <https://doi.org/10.1038/s41563-019-0367-7>.

Reprints and permissions information is available at www.nature.com/reprints.

Correspondence and requests for materials should be addressed to C.A.D.

Publisher's note: Springer Nature remains neutral with regard to jurisdictional claims in published maps and institutional affiliations.

© The Author(s), under exclusive licence to Springer Nature Limited 2019

Methods

Synthesis of polyglycine probes for sortagging. Polyglycine-containing peptides (H-GGGGDDK(N₃)-NH₂, H-GGGGDDK(CHO)-NH₂, H-GGGGDDK(oNB-N₃)-NH₂, H-GGGG-oNB-DDK(CHO)-NH₂) were synthesized through standard Fmoc solid-phase methodologies that involve a butyloxycarbonyl-protected N-terminal glycine and a 4-methyltrityl-protected C-terminal lysine residue. After the selective deprotection of 4-methyltrityl (1% trifluoroacetic acid (TFA) in dichloromethane) on the resin, azide (N₃), aldehyde (CHO) and photoreleasable azide (oNB-N₃) functionality were installed, respectively, by condensation with 4-azidobutanoic acid, 4-formylbenzoic acid or 4-(1-(4-azidobutanoyloxy)ethyl)-2-methoxy-5-nitrophenoxybutanoic acid and the ε-amino group of the C-terminal lysine. Resin was washed (dimethylformamide, three times, and dichloromethane, three times) prior to peptide cleavage/deprotection (95:5 TFA:H₂O, 20 ml, 2 h) and precipitation (diethyl ether, 180 ml, 0 °C, twice). The crude peptide was purified via semipreparative reversed-phase high-performance liquid chromatography using a 55 min gradient (5–100% of acetonitrile and 0.1% TFA in H₂O) and lyophilized to give the final product. Peptide purity was confirmed by matrix-assisted laser desorption/ionization time-of-flight mass spectrometry. The complete synthetic details and characterization are given in Supplementary Methods.

Generation of homogeneous protein–peptide conjugates by STEPL. STEPL plasmids for EGFP, mCherry, mCerulean, bla, EGF, FGF and EGFP-EGF were constructed from pSTEPL³⁷ using standard cloning techniques (Supplementary Methods) and transformed into BL21 (DE3) *Escherichia coli* (Thermo Fisher). For protein expression, transformants were grown at 37 °C in a lysogeny broth that contained ampicillin (100 µg ml⁻¹) until an optical density of 0.6 (λ = 600 nm). Expression was induced with isopropyl β-D-1-thiogalactopyranoside (0.5 mM) and then agitated overnight at 18 °C. Cells were collected via centrifugation and lysed by sonication. The clarified lysate was loaded onto HisPur Ni-NTA resin (ThermoFisher), which was washed (20 mM Tris, 50 mM NaCl and 20 mM imidazole) to remove unbound proteins. After treatment of the resin with the polyglycine probe of interest (20×, 4 h, 37 °C), sortagged proteins were eluted and purified by dialysis (molecular weight cutoff, ~10 kDa). The protein identity and purity were confirmed by liquid chromatography–tandem mass spectrometry, sodium dodecyl sulfate polyacrylamide gel electrophoresis and gel shift analysis. The protein concentrations were determined by UV absorption (λ = 280 nm) and bicinchoninic acid assay prior to use. The complete experimental details are given in Supplementary Methods.

Random modification of proteins by NHS chemistry. Statistically modified proteins were prepared by reacting N₃-OSu (0×, 0 µM; 10×, 300 µM; 100×, 3 mM; 1,000×, 30 mM) with protein (30 µM) in phosphate buffered saline (PBS) (900 µl) and dimethylformamide (100 µl) overnight at room temperature. The resulting protein solutions were purified with Zeba Spin Desalting Columns (molecular weight cutoff, ~7 kDa (Thermo Fisher)) and buffer exchanged into fresh PBS. Protein concentrations were determined by UV absorption (λ = 280 nm) and bicinchoninic acid assay prior to use.

Activity determination of native and modified proteins. EGFP, mCherry and mCerulean fluorescences were quantified on a fluorescent plate reader (EGFP, λ_{excitation} = 470 nm, λ_{emission} = 530 nm; mCherry, λ_{excitation} = 575 nm, λ_{emission} = 620 nm; mCerulean, λ_{excitation} = 430 nm, λ_{emission} = 475 nm). Bla enzymatic activity was measured through a chromogenic assay, whereby bla (1 ng) was incubated with nitrocefin (2 mM) in PBS (100 µl). Sample absorbance (λ_{abs} = 386 nm) was measured over time at 37 °C; the initial slope was calculated as a measure of the *k*_{cat} of the enzyme. To determine the EGF activity, HeLa cells that expressed EKAREV³⁸ were plated in a 96-well plate (5,000 cells well⁻¹) and allowed to attach overnight in DMEM (Life Technologies) supplemented with fetal bovine serum (FBS, 10%). Cells were transitioned to serum-free DMEM 16 h prior to imaging. Time-series images (20 s intervals) were acquired on a fluorescent confocal microscope (λ_{excitation} = 405 nm, 1% argon laser power; λ_{emission,CFP} = 450–484 nm, λ_{emission,YFP} = 520–524 nm) after stimulation with EGF (12.5 nM) in serum-free DMEM. The YFP/CFP FRET response ratio was calculated for each frame (ImageJ) and plotted over time. The relative activity of each EGF species was taken as the initial rate of change of the FRET response after EGF stimulation, normalized to native EGF. Alternatively, EGF activity was determined through a commercially available DNA synthesis assay (Click-iT Edu Alexa Fluor 488 (Thermo Fisher)). NIH 3T3 cells were placed in a 96-well plate (5,000 cells well⁻¹) and cultured overnight in DMEM that contained FBS (10%). The cells were washed with PBS (twice) and transferred to serum-free DMEM. After 1 d, the cells were transitioned to serum-free DMEM that contained 5-ethynyl-2'-deoxyuridine (10 µM) with or without EGF (100 ng ml⁻¹). After 2 d of culture, the cells were fixed in formaldehyde and processed following the kit manufacturer's recommendations. The relative activity of each EGF species was taken as the percentage of cells actively synthesizing DNA after the EGF stimulation, normalized to unmodified EGF. FGF activity was determined through a proliferation assay using a commercially available assay (Quant-iT PicoGreen (Thermo Fisher)) for the double-stranded DNA content. NIH 3T3 cells (5,000 cells well⁻¹) were cultured overnight in a 96-well plate in DMEM that contained FBS (10%) prior to being transferred to serum-free DMEM.

After 1 d, the cells were transferred to serum-free DMEM with or without FGF (100 ng ml⁻¹), incubated for 2 d and assayed following the manufacturer's protocol. The relative activity of each FGF species corresponds to the total double-stranded DNA content, normalized to unmodified FGF.

Formation of SPAAC-based hydrogels. A solution of PEG-tetraBCN (*M*_n ~20,000 Da, 4 mM), N₃-PEG-N₃ (*M*_n ~3,500 Da, 8 mM (Supplementary Methods)) and N₃-TEG-OH-NPPOC (0.1 mM) was prepared in PBS. The network formation was allowed to proceed for 1 h between Rain-X-treated glass slides with silicone rubber spacers (0.5 mm thick (McMaster-Carr)). The slides were separated, and gels were equilibrated overnight in PBS prior to use.

Photopatterning conditions for protein tethering and release. For photolithographic patterning, hydrogels were exposed to collimated UV light (λ = 365 nm, 10 mW cm⁻², 0–1,200 s) through a patterned chrome photomask (Photo Sciences) using a Lumen Dynamics OmniCure S1500 Spot UV Curing system equipped with an internal 365 nm band-pass filter and a second in-line 360 nm cut-on long-pass filter. Protein gradients were created by moving an opaque plate attached to a programmable linear motion stage over gels during light exposure at various rates (0.3–2.4 mm min⁻¹). For the 3D patterning experiments within gels, an Olympus FV1000 MPE BX61 Multi-photon Microscope with a ×20 objective was used. Regions of interest were scanned 16 times with pulsed laser light (λ = 740 nm, 50% laser power) with a 2.5 µm *z* interval to generate 3D patterns. After NPPOC cleavage, gels were incubated for 8 h with an aldehyde-tagged protein (100 µM in PBS) at room temperature and protected from light. To remove unbound protein, gels were gently agitated in PBS (16 h) prior to imaging. After light exposure, gels that contained photoreleasable proteins were incubated in PBS (16 h) prior to analysis. This process was repeated iteratively for the patterning of multiple proteins. Experiments that involved the patterning of fluorescent proteins were visualized by fluorescent confocal or multiphoton microscopy, whereas those that involved immobilized bla were imaged by phase contrast microscopy. For experiments that involved encapsulated mammalian cells, PBS was replaced with culture media during the gel formation and patterning.

Spatial assessment of bla enzymatic activity. SPAAC-based gels uniformly functionalized with bla-oNB-N₃ (30 µM) were subjected to masked light (λ = 365 nm, 10 mW cm⁻², 10 min). Protein-patterned gels were incubated with thioacetate cefalotin (5 mM (Supplementary Methods)) and phenazine methosulfate (6.5 mM) in PBS (37 °C, 1 h). The gels were then washed with PBS (three times, 15 min) prior to visualization by phase contrast microscopy.

Encapsulation of MAPK FRET reporter cells. HeLa cells stably transfected with the EKAREV FRET sensor³⁸ were expanded in high-glucose DMEM supplemented with FBS (10%) and penicillin/streptomycin (1%) in a 5% CO₂ atmosphere at 37 °C. The culture medium was changed every 2–3 d and cells were passaged at ~70% confluency. HeLa cells were encapsulated (2 × 10⁶ cells ml⁻¹) in SPAAC-based gels (10 µl) modified with EGF-oNB-N₃ (12.5 nM) and an N₃-GRGS-NH₂ peptide (100 µM (Supplementary Methods)) for cell attachment. Photopatterning was performed 24 h after the encapsulation. Prior to FRET imaging (16 h), the culture media was replaced with serum-free DMEM that contained penicillin/streptomycin (1%).

Visualization of patterned MAPK signalling. HeLa EKAREV-laden hydrogels were imaged using a Leica SP8X confocal microscope at a constant distance below the gel surface (100 µm). EKAREV was excited using an argon laser (λ = 405 nm, 10% laser power); CFP excitation was monitored from λ_{emission,CFP} = 450–484 nm, whereas YFP fluorescence was measured from λ_{emission,YFP} = 520–524 nm. After image acquisition, the background fluorescence was subtracted and the YFP/CFP ratio for each pixel of the image was calculated using ImageJ. FRET response ratios were visualized as a blue–green–red colour map.

Cell response to dynamically patterned EGFP-EGF. EGFP-EGF-oNB-N₃ (25 µM) was conjugated (25 °C, 1 h) to PEG-tetraBCN (*M*_n ~20,000 Da, 4 mM). EGFP-EGF-modified hydrogels (5 µl) were formed (1 h) between Rain-X-treated glass slides with silicone rubber spacers (0.5 mm thick (McMaster-Carr)) with cell adhesive and matrix metalloproteinase-degradable crosslinker N₃-GGRGDSPGGPQGIWGGQK(N₃)-NH₂ (8 mM (Supplementary Methods)). After removal from the glass slide chamber, the gels were exposed to masked collimated UV light (λ = 365 nm, 10 min, 10 mW cm⁻²) through a slitted photomask that contained 400 µm wide line features and then soaked in PBS overnight. The gels were swollen (1 h) in DMEM that contained FBS (10%) prior to cell seeding. A431 cells (1 × 10⁷ cells ml⁻¹) were added to the top of the gels as a droplet (10 µl) and allowed to attach (1 h, 37 °C) prior to media addition. The gels were swollen in DMEM that contained FBS (10%) and penicillin/streptomycin (1%) overnight prior to imaging (condition 1 (Fig. 6)). The gel media were supplemented with BSA, 0.1% and cells maintained in culture (37 °C, 5% CO₂). After 3 d, a portion of the hydrogels were exposed to a second round of photopatterning; one-half of each treated gel was exposed to UV light (λ = 365 nm, 10 min, 10 mW cm⁻²) and

the other half was left unexposed. In all cases, the gels were maintained in DMEM that contained FBS (10%), penicillin/streptomycin (1%) and BSA (0.1%) for an additional 3 d prior to analysis (conditions 2 and 3 (Fig. 6)). At the end of each treatment condition, cells were fixed in paraformaldehyde (1%, 30 min), stained with 4',6-diamidino-2-phenylindole (0.15 $\mu\text{g ml}^{-1}$, 30 min) and visualized via fluorescence microscopy. Image analysis was performed for each condition using ImageJ, quantifying the normalized intensity profile for EGFP, nuclei and optical transmission across the gel perpendicular to the photopatterned lines. Whole-gel images were performed on an Epson Perfection 4490 Photo document scanner.

Encapsulated cell response to subcellular photoreleased EGFP-EGF. A431 cells (2×10^6 cells ml^{-1}) were encapsulated in SPAAC hydrogels (5 μl) that contained EGFP-EGF-*o*NB- N_3 (125 nM) and the N_3 -GRGDS- NH_2 peptide (1 mM (Supplementary Methods)) affixed to an azide-functionalized slide (Supplementary Methods). The cells were cultured for 48 h in DMEM supplemented with FBS (10%) and penicillin/streptomycin (1%) before transferring to phenol red-free DMEM that contained FBS (10%) and penicillin/streptomycin (1%). The

protein photorelease was performed via multiphoton laser-scanning lithography (Olympus FV1000 MPE BX61 Multi-photon Microscope, $\times 20$ objective, $\times 5$ zoom, $\lambda = 740$ nm, 25% laser power, 16 scan repeats, z interval = 2.5 μm), confined to a $40 \mu\text{m} \times 30 \mu\text{m} \times 5 \mu\text{m}$ subvolume that bisects an individual cell. ImageJ was used to calculate the difference in EGFP fluorescence pixel intensity that accompanied the photorelease.

Statistics. Two-tailed t -tests assuming equal variance were performed to determine P values and statistical significance.

Reporting Summary. Further information on research design is available in the Nature Research Reporting Summary linked to this article.

Data availability

Plasmids and data that support the findings of this study are available from the corresponding author upon reasonable request.

Reporting Summary

Nature Research wishes to improve the reproducibility of the work that we publish. This form provides structure for consistency and transparency in reporting. For further information on Nature Research policies, see [Authors & Referees](#) and the [Editorial Policy Checklist](#).

Statistics

For all statistical analyses, confirm that the following items are present in the figure legend, table legend, main text, or Methods section.

n/a Confirmed

- The exact sample size (n) for each experimental group/condition, given as a discrete number and unit of measurement
- A statement on whether measurements were taken from distinct samples or whether the same sample was measured repeatedly
- The statistical test(s) used AND whether they are one- or two-sided
Only common tests should be described solely by name; describe more complex techniques in the Methods section.
- A description of all covariates tested
- A description of any assumptions or corrections, such as tests of normality and adjustment for multiple comparisons
- A full description of the statistical parameters including central tendency (e.g. means) or other basic estimates (e.g. regression coefficient) AND variation (e.g. standard deviation) or associated estimates of uncertainty (e.g. confidence intervals)
- For null hypothesis testing, the test statistic (e.g. F , t , r) with confidence intervals, effect sizes, degrees of freedom and P value noted
Give P values as exact values whenever suitable.
- For Bayesian analysis, information on the choice of priors and Markov chain Monte Carlo settings
- For hierarchical and complex designs, identification of the appropriate level for tests and full reporting of outcomes
- Estimates of effect sizes (e.g. Cohen's d , Pearson's r), indicating how they were calculated

Our web collection on [statistics for biologists](#) contains articles on many of the points above.

Software and code

Policy information about [availability of computer code](#)

Data collection

Data analysis

For manuscripts utilizing custom algorithms or software that are central to the research but not yet described in published literature, software must be made available to editors/reviewers. We strongly encourage code deposition in a community repository (e.g. GitHub). See the Nature Research [guidelines for submitting code & software](#) for further information.

Data

Policy information about [availability of data](#)

All manuscripts must include a [data availability statement](#). This statement should provide the following information, where applicable:

- Accession codes, unique identifiers, or web links for publicly available datasets
- A list of figures that have associated raw data
- A description of any restrictions on data availability

Field-specific reporting

Please select the one below that is the best fit for your research. If you are not sure, read the appropriate sections before making your selection.

- Life sciences Behavioural & social sciences Ecological, evolutionary & environmental sciences

For a reference copy of the document with all sections, see [nature.com/documents/nr-reporting-summary-flat.pdf](https://www.nature.com/documents/nr-reporting-summary-flat.pdf)

Life sciences study design

All studies must disclose on these points even when the disclosure is negative.

Sample size	All experiments were performed in biological triplicate.
Data exclusions	No data was excluded.
Replication	All attempts at replication were successful.
Randomization	Randomization was not performed, as it was deemed unnecessary for these studies.
Blinding	Blinding was not performed, as it was deemed unnecessary for these studies.

Reporting for specific materials, systems and methods

We require information from authors about some types of materials, experimental systems and methods used in many studies. Here, indicate whether each material, system or method listed is relevant to your study. If you are not sure if a list item applies to your research, read the appropriate section before selecting a response.

Materials & experimental systems

n/a	Involvement in the study
<input checked="" type="checkbox"/>	<input type="checkbox"/> Antibodies
<input type="checkbox"/>	<input checked="" type="checkbox"/> Eukaryotic cell lines
<input checked="" type="checkbox"/>	<input type="checkbox"/> Palaeontology
<input checked="" type="checkbox"/>	<input type="checkbox"/> Animals and other organisms
<input checked="" type="checkbox"/>	<input type="checkbox"/> Human research participants
<input checked="" type="checkbox"/>	<input type="checkbox"/> Clinical data

Methods

n/a	Involvement in the study
<input checked="" type="checkbox"/>	<input type="checkbox"/> ChIP-seq
<input checked="" type="checkbox"/>	<input type="checkbox"/> Flow cytometry
<input checked="" type="checkbox"/>	<input type="checkbox"/> MRI-based neuroimaging

Eukaryotic cell lines

Policy information about [cell lines](#)

Cell line source(s)	HeLa and A431 cells were purchased from ATCC and gifted by Dr. Suzie Pun (University of Washington). HeLa cells were purchased from the Japanese Cancer Research Resources Bank, stably transfected to express EKAREV FRET sensor, and gifted by Dr. Michiyuki Matsuda (Kyoto University).
Authentication	All cell lines were authenticated by suppliers (ATCC, Japanese Cancer Research Resources Bank).
Mycoplasma contamination	All cell lines used in these studies tested negative for mycoplasma contamination.
Commonly misidentified lines (See ICLAC register)	No commonly misidentified cell lines were used in these studies.